Monthly Notices
of the
ROYAL ASTRONOMICAL SOCIETY

MNRAS **491,** 3952–3966 (2020)
Advance Access publication 2019 November 28

doi:10.1093/mnras/stz3276

Non-stationary Antonov self-gravitating layer: analytics and numerics

Evgeny A. Malkov[1,2]★ and Alexey N. Kudryavtsev[1,3]

[1]*Khristianovich Institute of Theoretical and Applied Mechanics, Russian Academy of Sciences, Siberian Branch, 4/1 Institutskaya Str, 630090 Novosibirsk, Russia*
[2]*Siberian State University of Telecommunications and Information Sciences, 86 Kirova Str, 630102 Novosibirsk, Russia*
[3]*Department of Physics, Novosibirsk State University, 1 Pirogova Str, 630090 Novosibirsk, Russia*

Accepted 2019 November 14. Received 2019 November 7; in original form 2019 July 10

ABSTRACT

Large-scale instability of gravitating systems plays a key role in collisionless relaxation and in reaching a quasi-stationary state at the early stage of evolution. Advanced high-resolution methods and permanently increasing performance of computational systems allow this phenomenon to be studied by means of computer simulations at a new level. In this paper, an approach to verification and validation of computer codes implementing high-resolution methods is proposed. The approach is based on comparisons of the simulation results with exact non-stationary solutions of the Vlasov–Poisson equations. The evolution of the gravitating layer model is considered as an example of implementation of this approach. A one-parameter family of exact models of a non-stationary gravitating layer is described, and their stability to large-scale disturbances in the linear approximation is analytically studied. Non-linear instability development is computed with the use of the fifth-order conservative semi-Lagrangian WENO scheme.

Key words: gravitation – instabilities – methods: analytical – methods: numerical – galaxies: formation.

1 INTRODUCTION

In most problems associated with the formation and evolution of galaxies and galactic clusters, these objects can be considered as collisionless systems consisting of continuously distributed self-gravitating matter (Binney & Tremaine 2008). The dynamics of such systems is governed by the Vlasov–Poisson equations

$$\frac{\partial f}{\partial t} + \mathbf{u}\frac{\partial f}{\partial \mathbf{r}} - \frac{\partial \Phi}{\partial \mathbf{r}}\frac{\partial f}{\partial \mathbf{u}} = 0, \tag{1}$$

$$\frac{\partial}{\partial \mathbf{r}}\frac{\partial \Phi}{\partial \mathbf{r}} = 4\pi G \int f \mathrm{d}\mathbf{u}. \tag{2}$$

Here $f(t, \mathbf{r}, \mathbf{u})$ is the distribution function in the 6D phase space, which depends on the time t, position $\mathbf{r}$, and velocity $\mathbf{v}$, and $\Phi(t, \mathbf{r})$ is the gravitation potential.

The laws of long-time evolution of systems with long-range forces and, in particular, approaching the equilibrium state are not well understood. In the absence of collisions, processes that play a key role in reaching a close-to-equilibrium distribution are the phase mixing and the so-called *violent relaxation* (Lynden-Bell 1967; Nakamura 2000; Arad & Lynden-Bell 2005; Yamaguchi 2008; Joyce & Worrakitpoonpon 2011). The main tool for studying such dynamic processes is computer simulation.

The most popular numerical methods used to solve the Vlasov–Poisson equations are the N-body simulation methods, where the examined system is presented by a large number of model particles interacting with each other directly or through softened gravitational forces (see review by Trenti & Hut 2008). However, these methods have some drawbacks. The discretization of the distribution function in these methods leads to such effects as the Monte Carlo noise and to artificial two-body relaxation (see e.g. Theis 1998); in certain cases, these drawbacks may cause dramatic consequences for the dynamic behaviour of the system, leading it far from the exact solution.

A number of alternative numerical techniques were proposed, including the 'cloudy' Vlasov solver (Alard & Colombi 2005), 'waterbag' methods (see e.g. Colombi & Touma 2014), integer lattice dynamics (Syer & Tremaine 1995; Mocz & Succi 2017), and special methods for

★ E-mail: malkov@itam.nsc.ru

'cold' collisionless medium with a negligible local velocity dispersion (e.g. Hahn & Angulo 2016; Sousbie & Colombi 2016). Nevertheless, the most straightforward method to simulate the dynamics of a self-gravitating system avoiding the discrete noise is to solve the Vlasov–Poisson equations (1) and (2) directly on Euler grids in the multidimensional phase space with a finite-difference, finite-volume, finite-element, or spectral method. In the seminal work of Cheng & Knorr (1976), a simple and efficient finite-difference scheme based on the time-splitting procedure (Strang 1968) and the backward characteristics method was introduced. The backward characteristic method is the main ingredient of the so-called semi-Lagrangian schemes (Sonnendrücker et al. 1999), which admit an appreciably greater time-step in comparison with purely Eulerian methods. A great deal of work aimed at developing more accurate and more robust Vlasov solvers was performed during last two decades. In particular, conservative and positivity-preserving numerical methods were developed based on high-resolution shock-capturing schemes, which ensure accurate reproduction of the solution in the regions where it is smooth, simultaneously maintaining the monotonicity near discontinuities (Filbet, Sonnendrücker & Bertrand 2001; Carillo & Vecil 2007; Umeda 2008; Crouseilles, Respaud & Sonnendrücker 2009; Crouseilles, Mehrenberger & Sonnendrücker 2010; Qiu & Christlieb 2010; Qiu & Shu 2011; Tanaka et al. 2017). This list is by no means exhaustive; critical comparisons of some Vlasov solvers are presented, for instance, in Arber & Vann (2002) and Filbet & Sonnendrücker (2003); further references to recent developments can be found in Sousbie & Colombi (2016) and Colombi & Alard (2017).

The grid-based Vlasov solvers are rather expensive in terms of computer memory and processing time because the computational grid should contain approximately $N_x^D \cdot N_v^D$ cells, where N_x and N_v are the characteristic numbers of discretization elements per one dimension in the coordinate and velocity spaces, respectively, and D is the physical dimension of the problem. However, they are now used more and more actively owing to increasing availability of high-performance computational systems, in particular including graphics processing units (GPUs), which allow massive parallelization (Rocha Filho 2013). In the past, the high-resolution Vlasov solvers were mostly applied in plasma physics, but since recently they have been also used for simulating the evolution of self-gravitating systems (e.g. Yoshikawa, Yoshida & Umemura 2013; Colombi et al. 2015; Colombi & Alard 2017; Tanaka et al. 2017; Halle, Colombi & Peirani 2019). It can be expected that in the future their wide application will offer a possibility of solving fundamental problems of stellar dynamics at a new level of numerical computations.

The use of high-resolution shock-capturing schemes for simulating the processes of formation and long-time evolution of large-scale self-gravitating systems, however, involves certain specific problems primarily caused by the influence of numerical dissipation inherent in the numerical schemes on the solution. Accurate computations require the conservation laws to be satisfied and entropy behaviour to be controlled during the process to avoid any numerical artefacts as much as possible. The best method of determining the consistency of the numerical method to the posed problem and the accuracy of solving the problem is to compare the results of numerical simulations with particular analytical solutions if they are available. Fortunately, there are non-trivial non-stationary solutions of the Vlasov–Poisson equations in 2D, 4D, and 6D phase spaces, which were found (e.g. Antonov & Nuritdinov 1981; Malkov 1986a,b; Vietri 1990; and Nuritdinov 1995). Moreover (and this is important), stability of 4D and 6D solutions, which describe pulsating gravitating spheres, spheroids, and also circular and elliptical discs, was also studied in the above-cited publications.

The goals of our investigations are, first, verification and validation of numerical codes for solving the Vlasov–Poisson equations through comparisons of the computation results with the non-stationary analytical solutions mentioned above. Second, it is planned to study the non-linear evolution of instabilities found analytically in the linear approximation and their influence on the formation of the structure of a collisionless gravitating system. The computations of a model pulsating gravitating layer are presented in the paper. The 2D phase model considered in this study possesses the main features of 6D models, but its numerical implementation is much less expensive, which allows one to perform series of high-resolution computations within a comparatively short time and to work out the basic stages of the approach to computer simulations of 6D models.

The remaining part of the paper is arranged in the following way. The exact solution of the Vlasov–Poisson equations, representing a model pulsating gravitating layer, is given in Section 2. Section 3 describes a study of the stability of this model to large-scale perturbations. Section 4 deals with the numerical method used for the present computations, which is based on a fifth-order conservative WENO scheme; results of testing the code to be run on a GPU are also reported in Section 4. In Section 5, the results of the numerical simulations of the perturbation evolution are compared with analytical solutions that are stable in the linear approximation; the results of the numerical simulations of non-linear growth of perturbations that are unstable in the linear approximation are also reported.

2 EXACT SOLUTIONS OF THE VLASOV–POISSON EQUATIONS

A gravitating layer can be presented as a set of gravitationally interacting parallel planes with a homogeneous surface density. A continuum of such particles-planes is described by the kinetic Vlasov–Poisson equations, which are written in the case of a 2D phase space as

$$\frac{\partial f}{\partial t} + u\frac{\partial f}{\partial z} - \frac{\partial \Phi}{\partial z}\frac{\partial f}{\partial u} = 0, \tag{3}$$

$$\frac{\partial^2 \Phi}{\partial z^2} = 4\pi G \int f \,\mathrm{d}u, \tag{4}$$

where $f = f(t, u, z)$ is the phase density and $\Phi(t, z)$ is the potential (Camm 1950).

Malkov & Nuzhnova (2003) proposed a method of finding non-stationary solutions of the Vlasov–Poisson equations (1) and (2) based on the group analysis, described the known solutions by using a unified approach, and constructed a new phase model for a non-stationary self-gravitating spheroid. It was also demonstrated in the above-cited paper that equation (1) admits a group of differential transformations

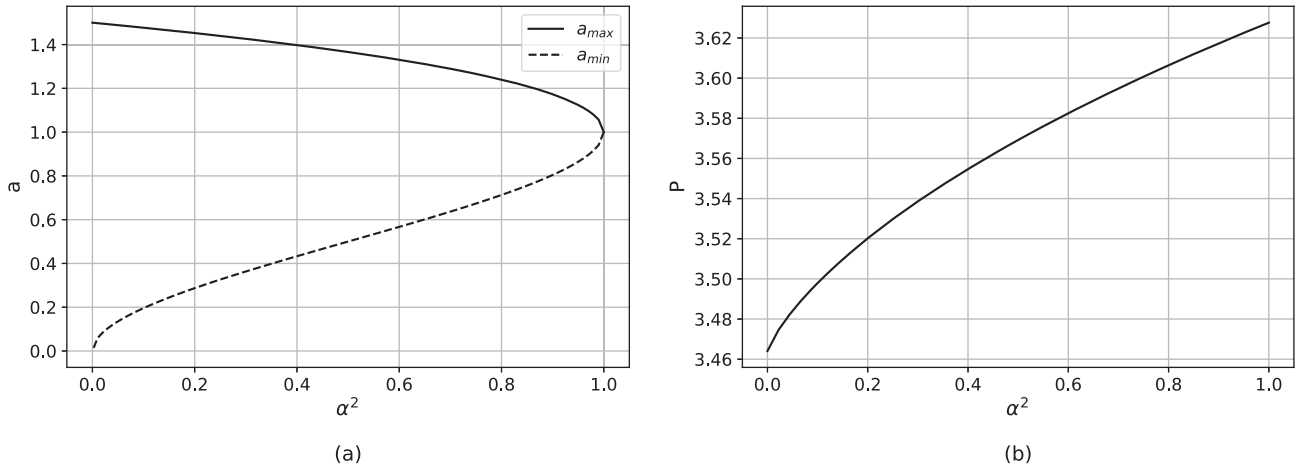

Figure 1. Maximum and minimum thicknesses of the pulsating layer (a) and period of pulsations (b) versus the parameter α^2.

only if the potential has a quadratic form and, thus, all possible non-stationary analytical solutions describe systems with a homogeneous spatial density. In particular, equations (3) and (4) have the solution

$$\Phi_0(t,z,u)=\frac{2\pi G\rho_0 z^2}{a}+\text{const}, \tag{5}$$

$$f_0=\frac{\rho_0}{\pi}\left[\alpha^2\left(z_0^2-\frac{z^2}{a^2}\right)-a^2\left(u-\frac{\dot a}{a}z\right)^2\right]^{-1/2}, \tag{6}$$

where the function $a=a(t)$ satisfies the equation

$$\ddot a=\frac{\alpha^2}{a^3}-1. \tag{7}$$

The proposed solution meant for studying the non-linear stability of a pulsating gravitating layer is parametrized in such a way that all models corresponding to different values of the parameter have an identical total energy and different final amplitudes of pulsations. Indeed, the kinetic energy of the layer is

$$E_{\rm kin}=\frac{1}{2}\int f(t,z,u)u^2\mathrm{d}u\mathrm{d}z=\frac{2}{3}\rho_0 z_0^3\left(\frac{\dot a^2}{2}+\frac{\alpha^2}{2a^2}\right), \tag{8}$$

and the potential energy is

$$W=\int f(t,z,u)z\frac{\partial\Phi}{\partial z}\mathrm{d}u\mathrm{d}z=\frac{2}{3}\rho_0 z_0^3 a. \tag{9}$$

Thus, the total energy of the layer with the distribution function (6) is

$$E_{\rm tot}=E_{\rm kin}+W=\frac{2}{3}\rho_0 z_0^3\left(\frac{\dot a^2}{2}+\frac{\alpha^2}{2a^2}+a\right). \tag{10}$$

Hereinafter, the unit time is taken to be $1/\sqrt{4\pi G\rho_0}$, i.e. $4\pi G\rho_0$ is assumed to be equal to unity. The expression in brackets in equation (10) is the first integral of equation (7) and is equal to a constant. Assuming it to be equal to 3/2, we obtain a family of gravitating layer models with an identical total energy and different values of the parameter α^2, which characterizes the degree of system unsteadiness. Indeed, the virial ratio for the model is expressed by the formula

$$R_{\rm vir}=\frac{2E_{\rm kin}}{W}=\frac{\alpha^2}{a^3}+\frac{\dot a^2}{a}, \tag{11}$$

and its value at the instant of the maximum and minimum compression ($\dot a=0$) is related to the parameter α^2 by a simple relation $\alpha^2=a^3R_{\rm vir}$. Fig. 1 shows the maximum and minimum thicknesses of the pulsating layer and the period of pulsations as functions of the parameter α^2.

To finalize the description of the undisturbed model of the pulsating layer, the following should be noted: passing to the variables

$$\hat z=z/a,\quad \hat u=a\left(u-\frac{\dot a}{a}z\right),\quad \hat t=\int\frac{\mathrm{d}t}{a^2}, \tag{12}$$

where the group of transformations admitted by the Vlasov–Poisson equations (3) and (4) is a group of parallel displacements along the new time variable $\hat t$ (Malkov & Nuzhnova 2003), we obtain an autonomous system of integro–differential equations. The distribution function (6)

in these variables is written as

$$f_0 = \frac{\rho_0}{\pi} \frac{1}{\sqrt{\alpha^2\left(z_0^2 - \hat{z}^2\right) - \hat{u}^2}}. \tag{13}$$

At $a(t) \equiv 1$, the distribution function (6) coincides with the distribution function for a stationary layer, which was obtained by Antonov (1971), who investigated its stability in linear approximation also. Therefore, solutions (5) and (6) can be considered as a generalized non-stationary Antonov solution. It should be noted that non-linear perturbations of the stationary layer, preserving its homogeneity, were studied by Kalnajs (1973).

3 LINEAR INSTABILITY OF PULSATING MODELS

Linearizing the collisionless kinetic equation (1), we obtain a system of linear integro–differential equations

$$\frac{\mathrm{D}f_1}{\mathrm{D}t} = \frac{\partial \Phi_1}{\partial u}\frac{\partial f_0}{\partial u}, \tag{14}$$

$$\frac{\partial^2 \Phi_1}{\partial z^2} = 4\pi G \int f_1 \mathrm{d}u, \tag{15}$$

where

$$\frac{\mathrm{D}}{\mathrm{D}t} = \frac{\partial}{\partial t} + u\frac{\partial}{\partial z} - \frac{\partial \Phi_0}{\partial z}\frac{\partial}{\partial u} \tag{16}$$

is the Lagrangian derivative along the undisturbed trajectory, along the characteristic of equation (3).

The distribution function in the new variables (13) with the phase domain boundary explicitly taken into account, where the function differs from zero, has the form

$$f_0 = \frac{\rho_0}{\pi} \frac{\Pi(\hat{u}, \hat{\kappa})}{\sqrt{\hat{\kappa}^2 - \hat{u}^2}}, \tag{17}$$

where $\hat{\kappa}^2 = \alpha^2\left(z_0^2 - \hat{z}^2\right)$, $\Pi(\hat{u}, \hat{\kappa}) = \theta(\hat{u} + \hat{\kappa}) - \theta(\hat{u} - \hat{\kappa})$ is a rectangular function, and $\theta(x)$ is the Heaviside function.

For the potential of systems with a homogeneous density and a distribution function of the form (13), the disturbance can be chosen in the form of polynomials in powers of spatial variables (in our case, in powers of $\hat{z}$). For studying the stability of individual modes, it is sufficient to keep terms of the polynomial of the corresponding power (Antonov 1971; Fridman & Polyachenko 1984). This property of the undisturbed potential is also valid for non-stationary models. Thus, the potential disturbance is sought in the form

$$\Phi_1(t, z) = z^n \phi(t)/a^m(t). \tag{18}$$

Then equations (14) and (15) in variables (12) under the condition that $m = n + 2$ are written as

$$\frac{\mathrm{D}f_1}{\mathrm{D}\hat{t}} = \frac{\rho_0}{\pi} n \hat{z}^{n-1}\hat{u}\phi \left\{ \frac{\Pi(\hat{u}, \hat{\kappa})}{[\hat{\kappa}^2 - \hat{u}^2]^{1.5}} - \frac{\delta(\hat{u} + \hat{\kappa}) + \delta(\hat{u} - \hat{\kappa})}{\hat{\kappa}\sqrt{\hat{\kappa}^2 - \hat{u}^2}} \right\}, \tag{19}$$

$$n(n-1)\hat{z}^{n-2}\frac{\phi}{a^3} = \int f_1 \mathrm{d}\hat{u}. \tag{20}$$

The particle trajectories, which are the characteristics of the collisionless kinetic Vlasov equation (3) written in variables (12), are

$$\begin{cases} \hat{z}' \equiv \hat{z}(\hat{t}') = \hat{z}\cos\alpha(\hat{t}' - \hat{t}) + \dfrac{1}{\alpha}\hat{u}\sin\alpha(\hat{t}' - \hat{t}), \\ \hat{u}' \equiv \hat{u}(\hat{t}') = -\alpha\hat{z}\sin\alpha(\hat{t}' - \hat{t}) + \hat{u}\cos\alpha(\hat{t}' - \hat{t}). \end{cases} \tag{21}$$

Integrating equation (19) along the trajectories (21), we obtain

$$f_1(\hat{t}, \hat{z}, \hat{u}) = \frac{\rho_0}{\pi} n \left\{ \frac{\Pi(\hat{u}, \hat{\kappa})}{[\hat{\kappa}^2 - \hat{u}^2]^{3/2}} - \frac{\delta(\hat{u} + \hat{\kappa}) + \delta(\hat{u} - \hat{\kappa})}{\hat{\kappa}\sqrt{\hat{\kappa}^2 - \hat{u}^2}} \right\} \int_{\hat{t}_0}^{\hat{t}} \hat{z}(\hat{t}')^{n-1}\hat{u}(\hat{t}')\phi(\hat{t}')\mathrm{d}\hat{t}'. \tag{22}$$

In writing equation (22), we used the invariance of the expression in curved brackets with respect to transformations (21). Substituting equation (22) into equation (20), we obtain the equation for an arbitrary disturbance mode

$$\frac{\phi(\hat{t})}{a(\hat{t})^3}\hat{z}^{n-2} = \frac{1}{\pi(n-1)} \int_{-\infty}^{\infty} \mathrm{d}\hat{u} \left\{ \left[\frac{\Pi(\hat{u}, \hat{\kappa})}{[\hat{\kappa}^2 - \hat{u}^2]^{3/2}} - \frac{\delta(\hat{u} + \hat{\kappa}) + \delta(\hat{u} - \hat{\kappa})}{\hat{\kappa}\sqrt{\hat{\kappa}^2 - \hat{u}^2}} \right] \int_{\hat{t}_0}^{\hat{t}} \hat{z}(\hat{t}')^{n-1}\hat{u}(\hat{t}')\phi(\hat{t}')\mathrm{d}\hat{t}' \right\}. \tag{23}$$

3.1 Potential perturbation $\sim z^2$

Let us first consider a perturbation that does not alter the density homogeneity. The higher term of the polynomial representing such a perturbation of the potential is written as

$$\Phi_1(t,z) = z^2\phi(t)/a(t)^3. \tag{24}$$

Equation (23) at $n = 2$ takes the form

$$\frac{\phi(\hat{t})}{a(\hat{t})^3} = \frac{1}{\pi}\int_{-\infty}^{\infty}\hat{u}^2\mathrm{d}\hat{u}\left\{\left[\frac{\Pi(\hat{u},\hat{\kappa})}{[\hat{\kappa}^2-\hat{u}^2]^{3/2}} - \frac{\delta(\hat{u}+\hat{\kappa})+\delta(\hat{u}-\hat{\kappa})}{\hat{\kappa}\sqrt{\hat{\kappa}^2-\hat{u}^2}}\right]\frac{1}{2\alpha}\int_{\hat{t}_0}^{\hat{t}}\sin 2\alpha(\hat{t}'-\hat{t})\phi(\hat{t}')\mathrm{d}\hat{t}'\right\}. \tag{25}$$

In writing equation (25), it was taken into account that the only term in the integrand of equation (23),

$$\hat{z}(\hat{t}')\hat{u}(\hat{t}') = \hat{z}^2(-\frac{1}{2}\sin 2\alpha\tau) + \hat{z}\hat{u}(\cos 2\alpha\tau) + \hat{u}^2\left(\frac{1}{2\alpha}\sin 2\alpha\tau\right), \tag{26}$$

which does not contain the power of $\hat{z}$, is proportional to $\hat{u}^2$ after integration with respect to $\hat{u}$. After calculating the integral

$$\int_{-\infty}^{\infty}\hat{u}^2\mathrm{d}\hat{u}\left[\frac{\Pi(\hat{u},\hat{\kappa})}{[\hat{\kappa}^2-\hat{u}^2]^{3/2}} - \frac{\delta(\hat{u}+\hat{\kappa})+\delta(\hat{u}-\hat{\kappa})}{\hat{\kappa}\sqrt{\hat{\kappa}^2-\hat{u}^2}}\right]$$

$$= \frac{\hat{u}}{\sqrt{\hat{\kappa}^2-\hat{u}^2}}\Big|_{\hat{u}=-\hat{\kappa}}^{\hat{u}=\hat{\kappa}} - \int_{-\hat{\kappa}}^{\hat{\kappa}}\frac{\mathrm{d}\hat{u}}{\sqrt{\hat{\kappa}^2-\hat{u}^2}} - \frac{\hat{u}^2}{\hat{\kappa}\sqrt{\hat{\kappa}^2-\hat{u}^2}}\Big|^{\hat{u}=-\hat{\kappa}} - \frac{\hat{u}^2}{\hat{\kappa}\sqrt{\hat{\kappa}^2-\hat{u}^2}}\Big|^{\hat{u}=\hat{\kappa}} = -\pi, \tag{27}$$

and substituting the result into equation (25), we finally obtain an integral equation for the function $\phi(\hat{t})$, which describes the behaviour of the potential perturbation $\sim z^2$:

$$\frac{\phi}{a^3} = -\frac{1}{2\alpha}\int_{\hat{t}_0}^{\hat{t}}\sin 2\alpha(\hat{t}'-\hat{t})\,\phi(\hat{t}')\,\mathrm{d}\hat{t}'. \tag{28}$$

Differentiating equation (28) twice, eliminating the integral, and applying the replacement $\psi = \phi/a^3$, we obtain the differential equation

$$\frac{\mathrm{d}^2\psi}{\mathrm{d}\hat{t}^2} + (4\alpha^2 - a^3)\psi = 0. \tag{29}$$

Passing to the independent time variable t related to $\hat{t}$ by the formula $\mathrm{d}t = a^2\mathrm{d}\hat{t}$, we obtain

$$\frac{\mathrm{d}^2\psi}{\mathrm{d}t^2} + 2\frac{\dot{a}}{a}\frac{\mathrm{d}\psi}{\mathrm{d}t} + \left(4\frac{\alpha^2}{a^4} - \frac{1}{a}\right)\psi = 0. \tag{30}$$

This derivation of equation (30) is universal and is used below to derive an evolutionary equation for the potential perturbation $\sim z^4$ violating the density homogeneity. Concerning the perturbation retaining the density homogeneity, it can be obtained in a simpler way. In this case, the disturbed layer behaviour also obeys equation (7). Let us write this perturbation in the form $a = a(1+\epsilon)$ and linearize this equation. The final equation is

$$\frac{\mathrm{d}^2\epsilon}{\mathrm{d}t^2} + 2\frac{\dot{a}}{a}\frac{\mathrm{d}\epsilon}{\mathrm{d}t} + \left(4\frac{\alpha^2}{a^4} - \frac{1}{a}\right)\epsilon = 0, \tag{31}$$

which coincides with equation (30). In the case of a stationary layer, the solution of equation (30) has the form

$$\psi(t) = c_1\exp\left(-i\sqrt{3}t\right) + c_2\exp\left(i\sqrt{3}t\right). \tag{32}$$

The solution coincides with the results of studying the stability of a stationary self-gravitating layer by Antonov (1971), who proved its stability to arbitrary perturbations.

3.2 Potential perturbation $\sim z^4$

The largest scale mode of the potential perturbation violating the spatial density homogeneity and triggering the mechanism of quasi-stationary structure formation in the case of instability is proportional to $\sim z^4$. Here, quasi-stationarity means stationarity of the phase density averaged over the cells of the phase space of a certain scale. The small-scale structure of the phase density always remains non-stationary by virtue of the Liouville theorem (e.g. Arnold 1980). This perturbation can be written in the form

$$\Phi_1(t,z) = z^4\phi(t)/a(t)^6. \tag{33}$$

The higher terms of the polynomial with respect to $\hat{z}$ in the right-hand side of equation (23) are identified by writing, similar to equation (26),

$$\begin{aligned}\hat{z}(\hat{t}')^3\hat{u}(\hat{t}') = {} & \hat{z}^4\left(-\alpha\cos^3\alpha\tau\sin\alpha\tau\right) + \hat{z}^3\hat{u}\left(\cos^4\alpha\tau - 3\cos^2\alpha\tau\sin^2\alpha\tau\right)\\ & + \hat{z}^2\hat{u}^2\frac{3}{4\alpha}\sin 4\alpha\tau + \hat{z}\hat{u}^3\frac{1}{\alpha^2}\left(3\cos^2\alpha\tau\sin^2\alpha\tau - \sin^4\alpha\tau\right)\\ & + \hat{u}^4\frac{1}{4\alpha^3}\left(\sin 2\alpha\tau - \frac{1}{2}\sin 4\alpha\tau\right).\end{aligned} \tag{34}$$

Here, $\tau = \hat{t}' - \hat{t}$. After integration with respect to $\hat{u}$ in equation (22), only terms proportional to $\hat{z}^2\hat{u}^2$ and $\hat{u}^4$ yield terms containing $\hat{z}^2$. Namely,

$$\begin{aligned}&\int\limits_{-\infty}^{\infty}\hat{u}^4\mathrm{d}\hat{u}\left[\frac{\Pi(\hat{u},\hat{\kappa})}{[\hat{\kappa}^2-\hat{u}^2]^{3/2}} - \frac{\delta(\hat{u}+\hat{\kappa})+\delta(\hat{u}-\hat{\kappa})}{\hat{\kappa}\sqrt{\hat{\kappa}^2-\hat{u}^2}}\right]\\ &= \frac{1}{2}\hat{u}\sqrt{\hat{\kappa}^2-\hat{u}^2}\Big|_{\hat{u}=-\hat{\kappa}}^{\hat{u}=\hat{\kappa}} + \frac{\hat{\kappa}^2\hat{u}}{\sqrt{\hat{\kappa}^2-\hat{u}^2}}\Big|_{\hat{u}=-\hat{\kappa}}^{\hat{u}=\hat{\kappa}} - \frac{3}{2}\hat{\kappa}^2\int\limits_{-\hat{\kappa}}^{\hat{\kappa}}\frac{\mathrm{d}\hat{u}}{\sqrt{\hat{\kappa}^2-\hat{u}^2}}\\ &\quad - \frac{\hat{u}^4}{\hat{\kappa}\sqrt{\hat{\kappa}^2-\hat{u}^2}}\Big|^{\hat{u}=-\hat{\kappa}} - \frac{\hat{u}^4}{\hat{\kappa}\sqrt{\hat{\kappa}^2-\hat{u}^2}}\Big|^{\hat{u}=\hat{\kappa}} = -\frac{3}{2}\hat{\kappa}^2\pi = -\frac{3}{2}\alpha^2\left(z_0^2-\hat{z}^2\right)\pi.\end{aligned} \tag{35}$$

Substituting equation (34) into equation (22), taking into account equations (27) and (35), and comparing terms at $\hat{z}^2$ in the resultant equation, we obtain the integral equation for the function ϕ

$$\frac{\phi(\hat{t})}{a(\hat{t})^3} = \frac{1}{8\alpha}A(\hat{t}) - \frac{5}{16\alpha}B(\hat{t}), \tag{36}$$

where

$$\begin{cases} A(\hat{t}) = \displaystyle\int\limits_{\hat{t}_0}^{\hat{t}}\sin 2\alpha(\hat{t}'-\hat{t})\,\phi(\hat{t}')\,\mathrm{d}\hat{t}', \\ B(\hat{t}) = \displaystyle\int\limits_{\hat{t}_0}^{\hat{t}}\sin 4\alpha(\hat{t}'-\hat{t})\,\phi(\hat{t}')\,\mathrm{d}\hat{t}'. \end{cases} \tag{37}$$

Differentiating equation (36) four times, we obtain a system of independent linear equations with respect to the unknowns $A(\hat{t})$ and $B(\hat{t})$:

$$\begin{cases} -\dfrac{\alpha}{2}A(\hat{t}) + 5\alpha B(\hat{t}) = \dfrac{\mathrm{d}^2}{\mathrm{d}\hat{t}^2}\dfrac{\phi}{a^3} - \phi, \\ 2\alpha^3 A(\hat{t}) - 80\alpha^3 B(\hat{t}) = \dfrac{\mathrm{d}^4}{\mathrm{d}\hat{t}^4}\dfrac{\phi}{a^3} - \dfrac{\mathrm{d}^2\phi}{\mathrm{d}\hat{t}^2} + 19\alpha^2\phi. \end{cases} \tag{38}$$

Solving system (38), substituting the solution into equation (36), and replacing the variables $\psi = \phi/a^3$, we obtain a differential equation with respect to the function $\psi(\hat{t})$ instead of the integral equation:

$$\frac{\mathrm{d}^4\psi}{\mathrm{d}\hat{t}^4} + \frac{\mathrm{d}^2}{\mathrm{d}\hat{t}^2}\left(20\alpha - \psi a^3\right) + \alpha a^3\left(64\frac{\alpha^2}{a^3} + 19\alpha - 20\right)\psi = 0. \tag{39}$$

For a stationary layer where $\alpha^2 = 1$ and $a(t) = 1$, equation (39) takes the form

$$\frac{\mathrm{d}^4\psi}{\mathrm{d}t^4} + 19\frac{\mathrm{d}^2\psi}{\mathrm{d}t^2} + 63\psi = 0, \tag{40}$$

and has the solution $\psi(t) \propto \exp(-\omega t)$, where the frequency ω is found from the equation

$$\omega^4 - 19\omega^2 + 63 = 0. \tag{41}$$

Thus, we have

$$\omega = \pm\sqrt{\frac{19 \pm \sqrt{109}}{2}}, \tag{42}$$

or, approximately,

$$\omega \approx \begin{cases} \pm 3.837, \\ \pm 2.069, \end{cases} \tag{43}$$

Table 1. Floquet multipliers.

α^2	$a_{\max}$	Period	Characteristic multiplier #1	Characteristic multiplier #2	Characteristic multiplier #3	Characteristic multiplier #4
1.00	1.000	3.62760	0.342 + 0.940i(1.000)	0.342 − 0.940i(1.000)	0.217 + 0.976i(1.000)	0.217 − 0.976i(1.000)
0.99	1.057	3.62659	0.332 + 0.943i(1.000)	0.332 − 0.943i(1.000)	0.236 + 0.972i(1.000)	0.236 − 0.972i(1.000)
0.98	1.080	3.62558	0.314 + 0.949i(1.000)	0.314 − 0.949i(1.000)	0.261 + 0.965i(1.000)	0.261 − 0.965i(1.000)
0.97	**1.097**	**3.62456**	**0.301 + 0.987i(1.032)**	**0.301 − 0.987i(1.032)**	**0.283 + 0.927i(0.969)**	**0.283 − 0.927i(0.969)**
0.96	1.111	3.62353	0.311 + 1.007i(1.054)	0.311 − 1.007i(1.054)	0.280 + 0.907i(0.949)	0.280 − 0.907i(0.949)
–	–	–	–	–	–	–
0.85	1.209	3.61190	0.397 + 1.095i(1.165)	0.397 − 1.095i(1.165)	0.293 + 0.807i(0.859)	0.293 − 0.807i(0.859)
–	–	–	–	–	–	–
0.50	1.366	3.56918	0.739 + 1.171i(1.385)	0.739 − 1.171i(1.385)	0.386 + 0.611i(0.722)	0.386 − 0.611i(0.722)
–	–	–	–	–	–	–
0.12	1.472	3.50284	1.614 + 0.335i(1.648)	1.614 − 0.335i(1.648)	0.594 + 0.123i(0.607)	0.594 − 0.123i(0.607)
0.11	1.474	3.50043	1.786	1.527	0.655	0.560
0.10	1.477	3.49795	2.105	1.293	0.773	0.475
–	–	–	–	–	–	–
0.07	1.484	3.48998	2.716	0.988 + 0.157i(1.000)	0.988 − 0.157i(1.000)	0.36822
–	–	–	–	–	–	–
0.01	1.498	3.46959	4.285	0.988 + 0.153i(1.000)	0.988 − 0.153i(1.000)	0.23334

which is consistent with the results obtained by Antonov (1971). Passing to the variable t, we write equation (39) as a system of differential equations of the form

$$\begin{cases} \dfrac{\mathrm{d}\psi}{\mathrm{d}t} = \dfrac{\psi_1}{a^2}, \\ \dfrac{\mathrm{d}\psi_1}{\mathrm{d}t} = \dfrac{\psi_2}{a^2}, \\ \dfrac{\mathrm{d}\psi_2}{\mathrm{d}t} = \dfrac{\psi_3}{a^2}, \\ \dfrac{\mathrm{d}\psi_3}{\mathrm{d}t} = -a\left(20\dfrac{\alpha^2}{a^3} - 1\right)\psi_2 + 6a^2\left(3 - \dfrac{\alpha^2}{a^2} - 2a\right)^{1/2}\psi_1 - \left[\alpha^2 a\left(64\dfrac{\alpha^2}{a^3} - 1\right) + 3a^4\left(3\dfrac{\alpha^2}{a^3} - \dfrac{12}{a} + 9\right)\right]\psi. \end{cases} \tag{44}$$

When equation (39) was transformed to system (44), equation (7) and its first integral were used.

For a stationary layer, the solution of equation (44) with the initial conditions $\psi = (1.0, 0.0, 0.0, 0.0)$ yields the expressions for the density perturbation:

$$\psi(t) \approx -0.410\cos(3.837\,t) + 1.410\cos(2.069\,t). \tag{45}$$

3.3 Linear analysis of perturbations

Equations (30) and (44) are linear equations with periodic coefficients. The qualitative character of the solution of such equations is determined by the eigenvalues of the fundamental matrix solution at the time $t = P$, where P is the period of the coefficients of the equation, with the initial condition equal to a unit matrix $\mathbf{M}(0) = \mathbf{I}$. The matrix $\mathbf{M}(P)$ is called the monodromy matrix, and the eigenvalues are called the Floquet multipliers. The details of the Floquet theory can be found, e.g. in Iooss & Joseph (1980).

To analyse the stability, it is sufficient to know that unbounded exponential growth of the solution of the system of linear equations with periodic coefficients should be expected if the absolute value of at least one multiplier is greater than unity. If the multipliers are real and equal to unity, then a linearly growing solution is obtained. The system has bounded quasi-periodic solutions if all multipliers are complex conjugate numbers with the absolute value equal to unity.

For equation (30), both multipliers are real and equal to unity for all values of the parameter α^2. Thus, in the linear approximation, the gravitating layer becomes unstable to perturbations retaining the homogeneous spatial density for all pulsation amplitudes. The instability has a power-law (in particular, linear) character. Its development does not lead to structural changes; the perturbed solution can be considered as pulsations of the homogeneous layer with a changed phase or amplitude. It is of interest to consider perturbations that change the spatial density. It should be expected that the most 'dangerous' mode that is unstable at lower densities of pulsations is the largest scale mode (33). The development of such a perturbation can lead to the formation of a quasi-stationary structure.

The Floquet multipliers of system (44) are listed in Table 1. The first three columns in the table provide information about the model family parameter α^2 associated with the virial ratio at the points where the layer pulsations stop, the maximum value of the function $a(t)$ defining the maximum thickness of the layer, and the period of layer pulsations, respectively. Instability emerges at $\alpha^2 \approx 0.97$. As an illustration, Fig. 2 shows the solutions of system (44) with the initial values (1.0, 0.0, 0.0, 0.0) for $\alpha^2 = 1.00$, 0.99, 0.98, and 0.96 corresponding to stable and exponentially unstable perturbations.

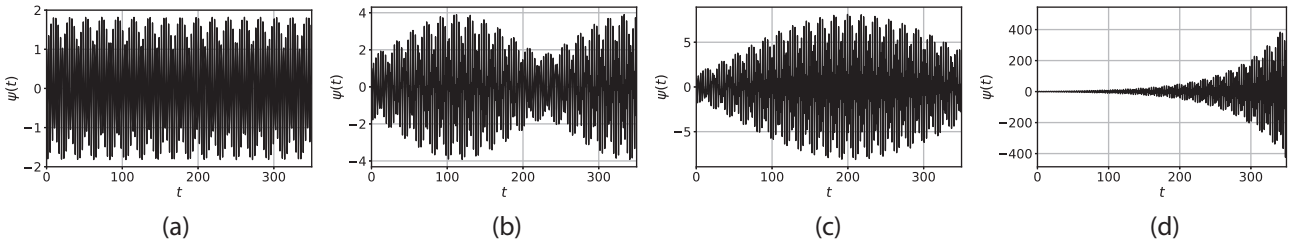

Figure 2. Behaviour of small perturbations $\Phi \sim z^4$ of the stationary layer (a) and for unstationary ones with $\alpha^2 = 0.99$ (b), 0.98 (c), and 0.96 (d).

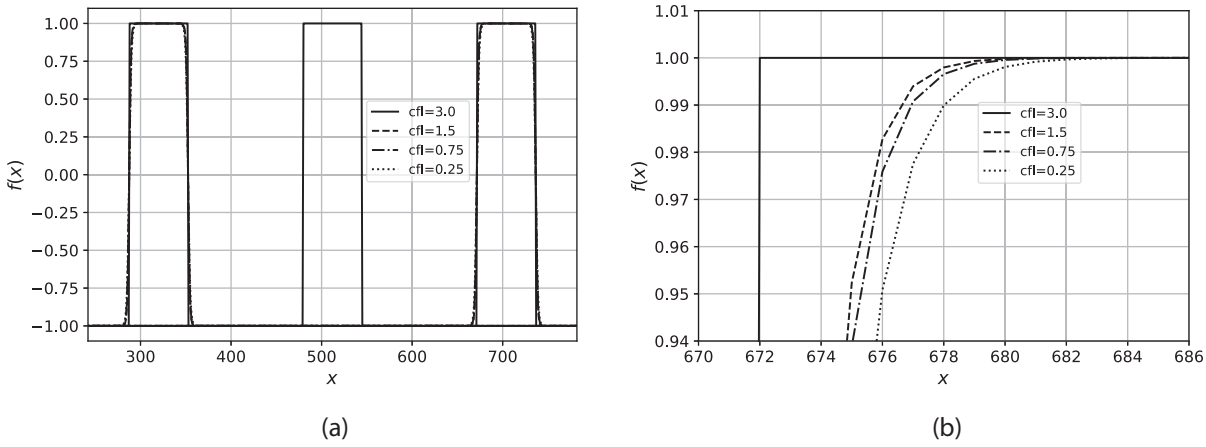

Figure 3. Computed advection of a rectangular function for different Courant numbers (a) and an enlarged fragment of the computed distributions (b).

4 NUMERICAL METHOD

The evolution of instability at the non-linear stage was numerically simulated with the use of the fifth-order conservative semi-Lagrangian WENO scheme (Qiu & Shu 2011). Multidimensional computations were performed with the second-order direction splitting scheme (Strang 1968). The most time-consuming parts of the code were parallelized to be executed on GPUs.

For verification of the developed code, computations of advection in a 1D and 2D space with a constant velocity field were performed. Fig. 3 (a) shows the computed advection of a rectangular distribution for different Courant numbers, $cfl = u\tau/h = 0.25$, 0.75, 1.5, and 3.0, where u is the constant advection velocity, τ is the time-step, and h is the step in space. The computational grid contains 1024 nodes. The plot in Fig. 3 (b) shows a fragment of the distribution, which allows one to evaluate the degree of dissipation in computations with different Courant numbers.

Figs 4 and 5 show the phase density contours obtained by means of the numerical solution of the 2D transport equation

$$\frac{\partial f}{\partial t} + u\frac{\partial f}{\partial z} + F(z)\frac{\partial f}{\partial u} = 0. \tag{46}$$

The computations were performed for two types of a stationary phase flow: linear flow $(u, -z)$ leading to rotation of the phase plane and non-linear flow $(u, -z - z^2)$ leading to rotation and deformation. The computational grid size was 2048 × 2048, the number of iterations was 6000, and the Courant number was $cfl = u_{\max}\tau/h = 0.75$. The computational domain in the phase space was $(u, z) \in [-2.0, 2.0] \times [-2.0, 2.0]$. The initial condition was a homogeneous phase density inside a $[-1.0, 1.0] \times [-1.0, 1.0]$ square.

Fig. 4 shows the contour of the initial phase density and the contours of the phase density changing under the action of a linear phase flow after 480 and 780 iterations. Fig. 5 shows the contours of the phase density changing under the action of a non-linear phase flow after 300, 1500, and 5100 iterations. It is seen that the WENO scheme ensures the absence of oscillations, whereas the high order of approximation and the semi-Lagrangian approach ensure low numerical dissipation.

5 NON-LINEAR EVOLUTION OF PERTURBATIONS

A conservative semi-Lagrangian scheme was used for computing the evolution of a pulsating gravitating layer for the numerical solution of the collisionless kinetic equation (3). Verification of this scheme was described in the previous paragraph. The computational grid contained 2048 × 2048 nodes. The computations were performed with different values of the Courant number for the unit velocity $u = 1.0$ and $cfl_1 = \tau/h$. The results were approximately identical in the interval from 0.1 to 1.0. The results of the computations for $cfl_1 = 1.0$ are reported in this

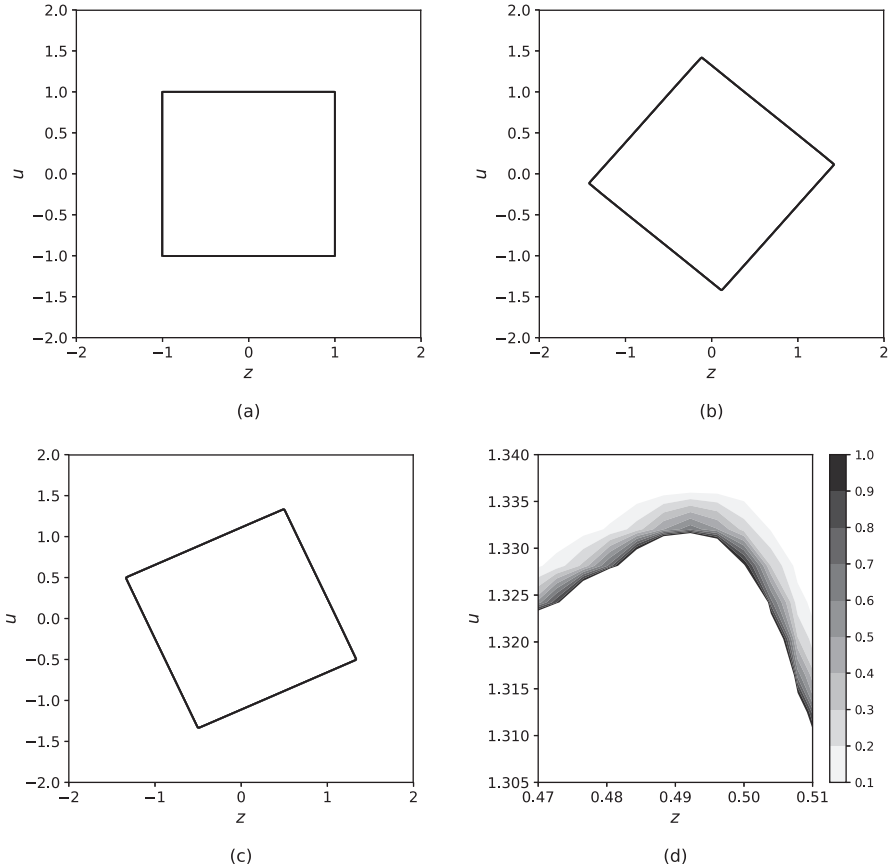

Figure 4. Evolution of a rectangular domain under the action of a linear phase flow. Phase density contours at initial time moment (a), after 480 (b) and 780 (c) iterations, an enlarged fragment of the density distribution after 780 iterations (d).

paper. The number of iterations was 60 000, which corresponded to slightly different values of physical time in different models. The force $F(z)$ was found by means of direct integration of the Poisson equation (2):

$$F(z) = -\frac{\partial \Phi}{\partial z} = 4\pi G \left[-\frac{1}{2} \int_{-\infty}^{z} \rho(\xi) \mathrm{d}\xi + \frac{1}{2} \int_{z}^{\infty} \rho(\xi) \mathrm{d}\xi \right]. \tag{47}$$

Fig. 6 illustrates the variation of the spatial density of the pulsating layer corresponding exactly to (5) and (6), and numerical solutions with the parameter $\alpha^2 = 0.98$. Excellent agreement can be noted.

The authors of this paper performed a series of computations of various models of gravitating layer pulsations for different values of α^2 and for the initial perturbation of the spatial density $\rho_1 \sim (a_0^2 - z^2)$, which corresponds to the perturbation of the potential $\Phi \sim z^4$. An important confirmation of the numerical scheme adequacy is the results computed for the values of the parameter $\alpha^2 = 0.98$, 0.96 at the stability region boundary with respect to the perturbations of $\Phi \sim z^4$ (see Table 1). Instability can be evidenced by the change in the amplitude of virial ratio pulsations accompanying instability development, whereas relaxation is expected to ensure reaching the asymptotic value $R_{\mathrm{vir}} = 1.0$.

Fig. 7 shows the variation of the virial ratio for models with the boundary values of $\alpha^2 = 0.98$ and 0.96. The density profiles formed after dozens of layer pulsations for the same parameters are plotted in Fig. 8. These figures clearly display the difference in the behaviour of the models corresponding to stable and unstable approximate solutions of the Vlasov–Poisson equations in the linear approximation. As an illustration, Figs 9 and 10 show the phase densities for the boundary values of the parameter $\alpha^2 = 0.98$ and $\alpha^2 = 0.96$, respectively.

The greater the unsteadiness of the gravitating system, the greater the value of the parameter α^2 characterizing this unsteadiness; moreover, the greater the linear instability increment (see Table 1), the sooner the formation of a quasi-stationary structure at the non-linear stage of instability development should be expected. To study the overall pattern of the gravitating layer structure being formed as a result of instability development, computations with $\alpha^2 = 0.5$ were performed. The number of iterations in these computations was increased to 120 000.

Fig. 11 illustrates the variation of the virial ratio during the time $t = 640$ or after 180 pulsations of the layer. Spatial density profiles at the initial stage of instability development approximately after 15 pulsations of the layer, at the stage of stabilization of the virial ratio amplitude approximately after 90 pulsations of the layer, and at a much later stage of layer evolution approximately

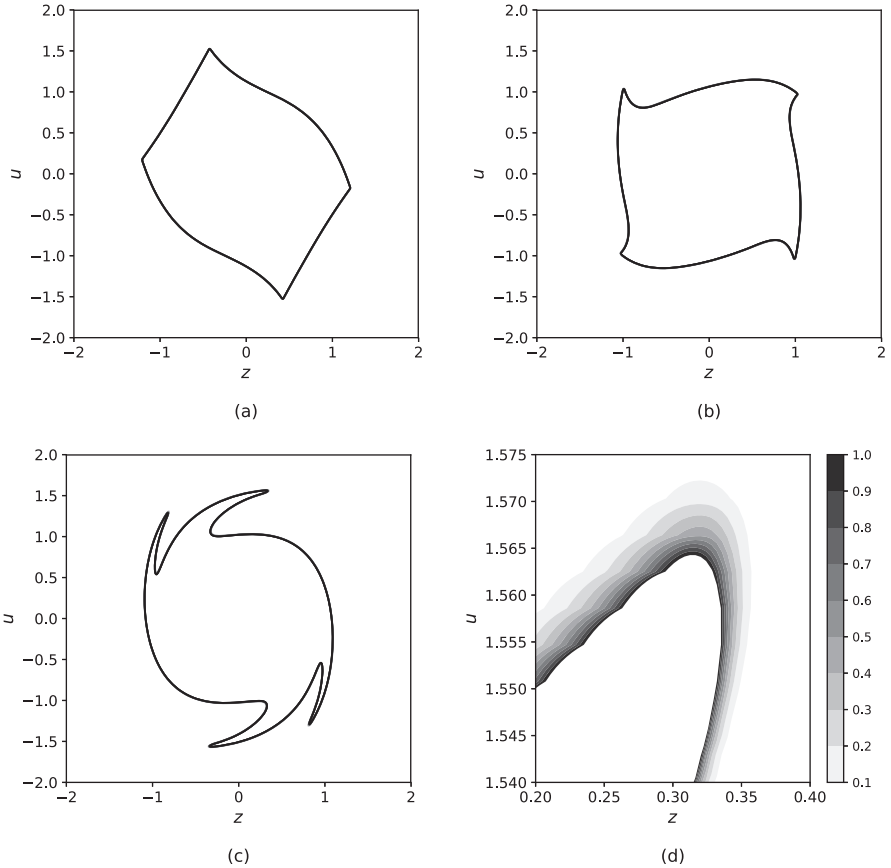

Figure 5. Evolution of a rectangular domain under the action of a nonlinear phase flow. Phase density contours after 300 (a), 1500 (b) and 5100 (c) iterations, an enlarged fragment of the density distribution after 5100 iterations (d).

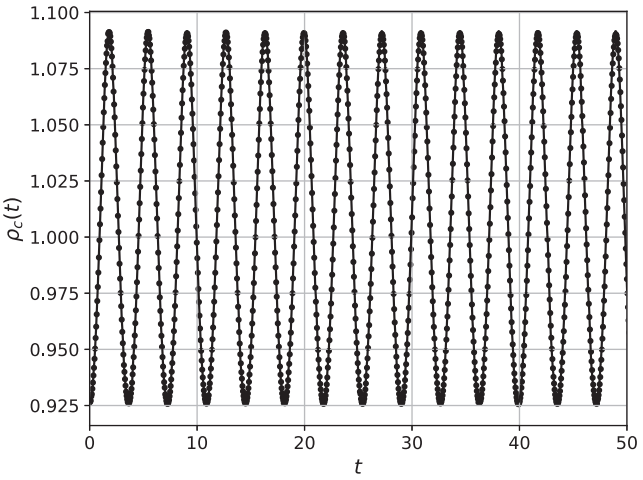

Figure 6. Comparison of the analytical (solid line) and numerical (circle markers) solutions for the pulsations of a homogeneous gravitating layer at $\alpha^2 = 0.98$.

after 180 pulsations are plotted, respectively, in Figs 12 (a), (b), (c). Phase densities images corresponding to these stages are shown in Figs 13–15.

It should be noted that the mass was exactly conserved during 120 000 iterations, which is natural in the case of using a conservative scheme, whereas the energy changes within one per cent.

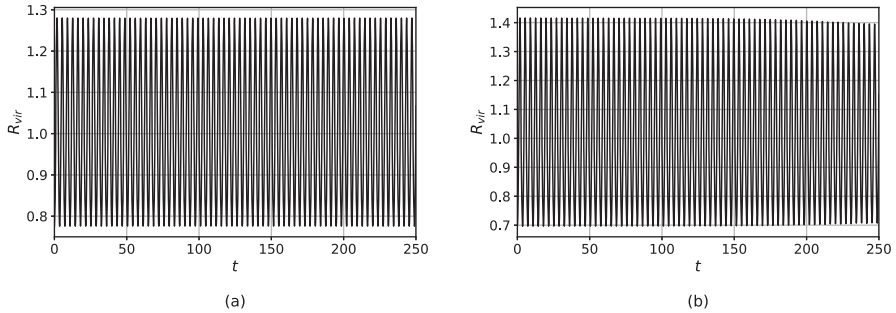

Figure 7. Amplitude of virial ratio pulsations for stable $\alpha^2 = 0.98$ (a) and unstable $\alpha^2 = 0.96$ (b) pulsations of the layer.

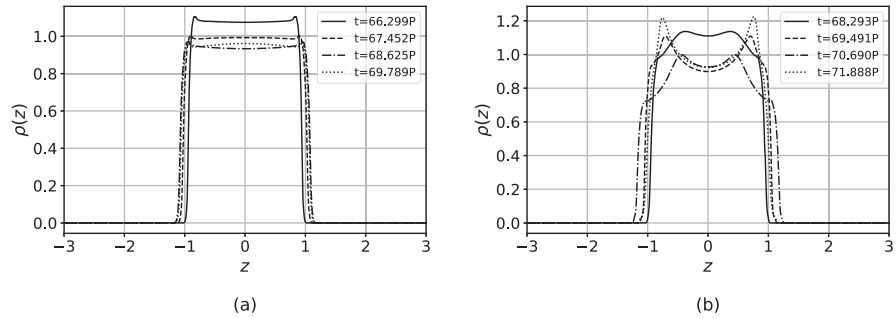

Figure 8. Density profiles for stable $\alpha^2 = 0.98$ (a) and unstable $\alpha^2 = 0.96$(b) pulsations of the layer. P is the pulsation period (see Table 1).

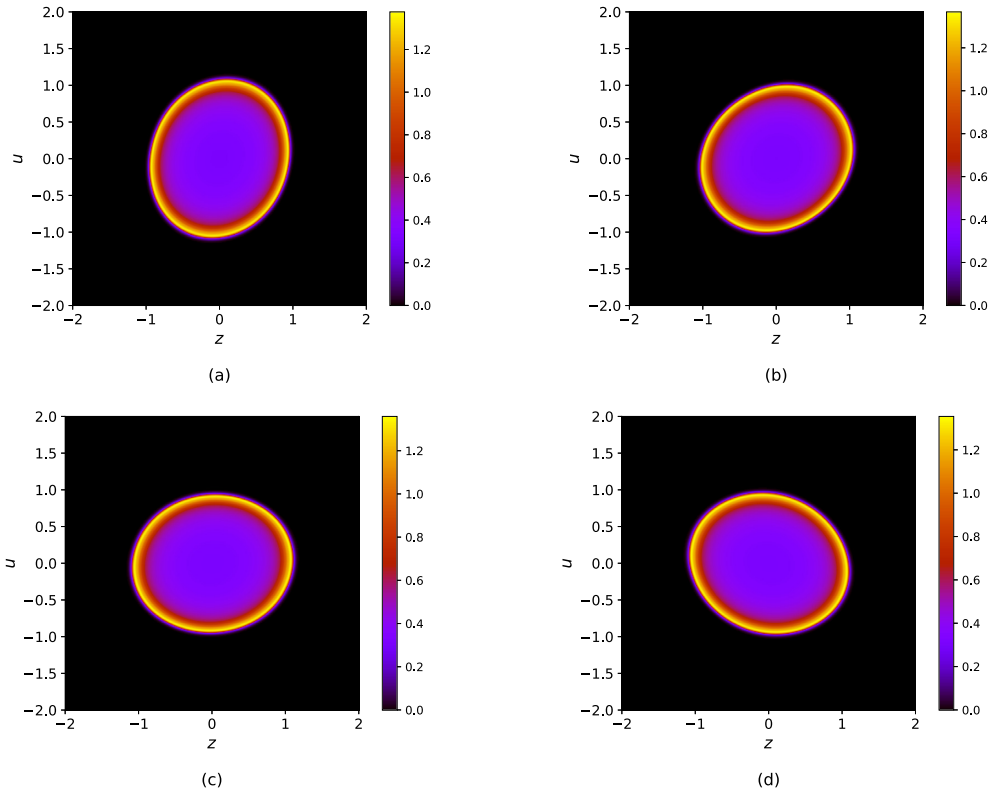

Figure 9. Phase density of stable solution ($\alpha^2 = 0.98$) at $t/P = 66.299$ (a), 67.462 (b), 68.625 (c), and 69.78 (d).

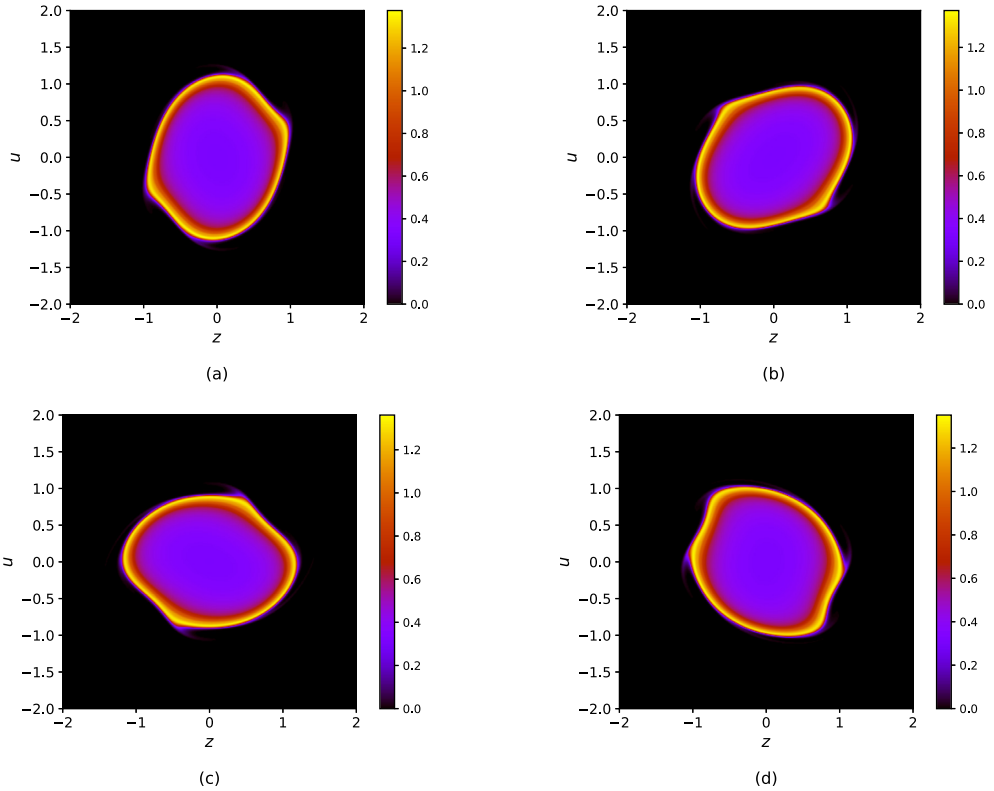

Figure 10. Onset of instability development for $\alpha^2 = 0.96$. Phase density at $t/P = 68.293$ (a), 69.491 (b), 70.690 (c), and 71.888 (d).

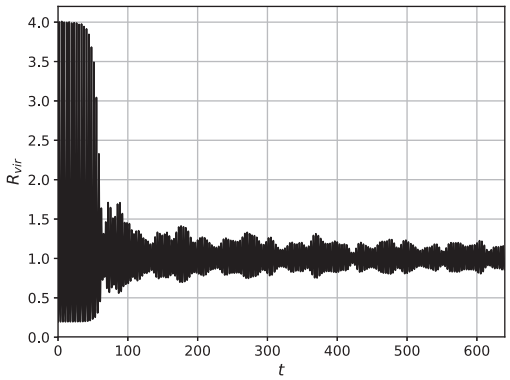

Figure 11. Evolution of the virial ratio amplitude for $\alpha^2 = 0.5$ over the time interval $t = 180\ P = 640$.

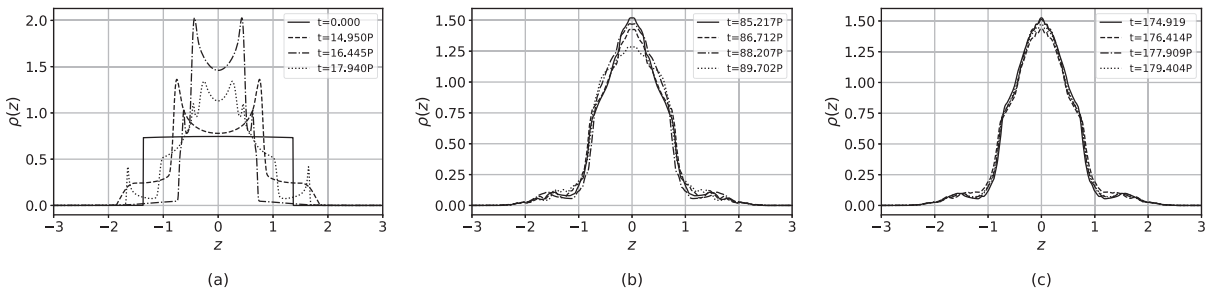

Figure 12. The spatial density profiles for $\alpha^2 = 0.5$.

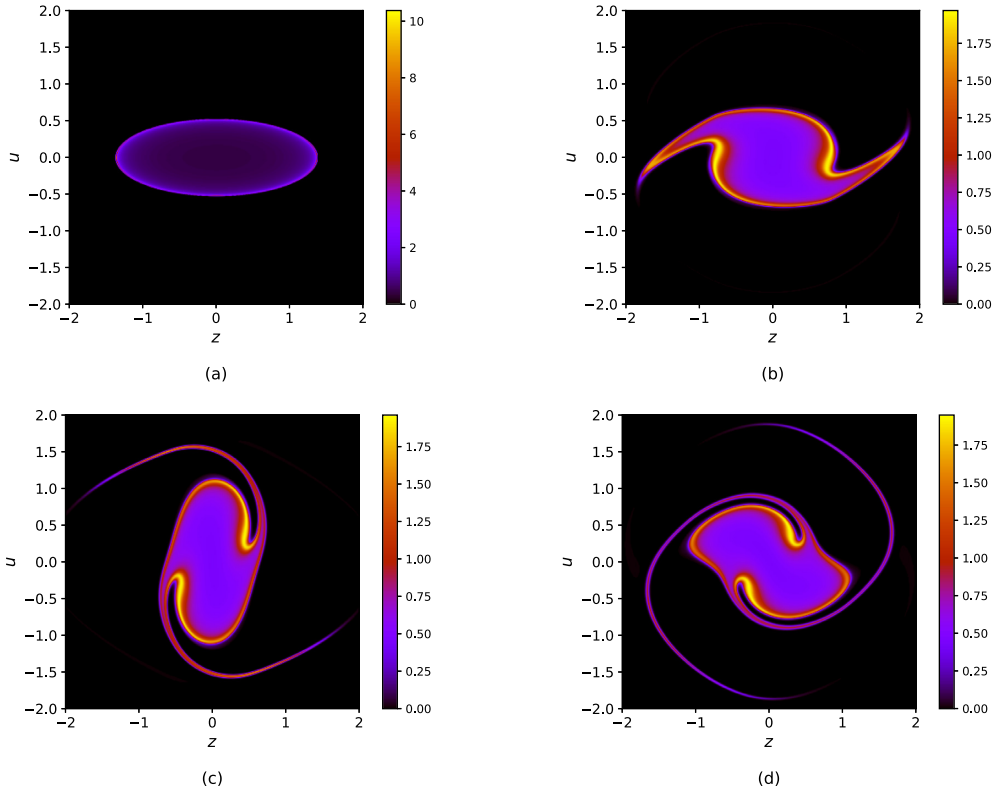

Figure 13. Phase density for $\alpha^2 = 0.5$ at $t/P = 0$ (a), 14.950 (b), 16.445 (c), and 17.940 (d).

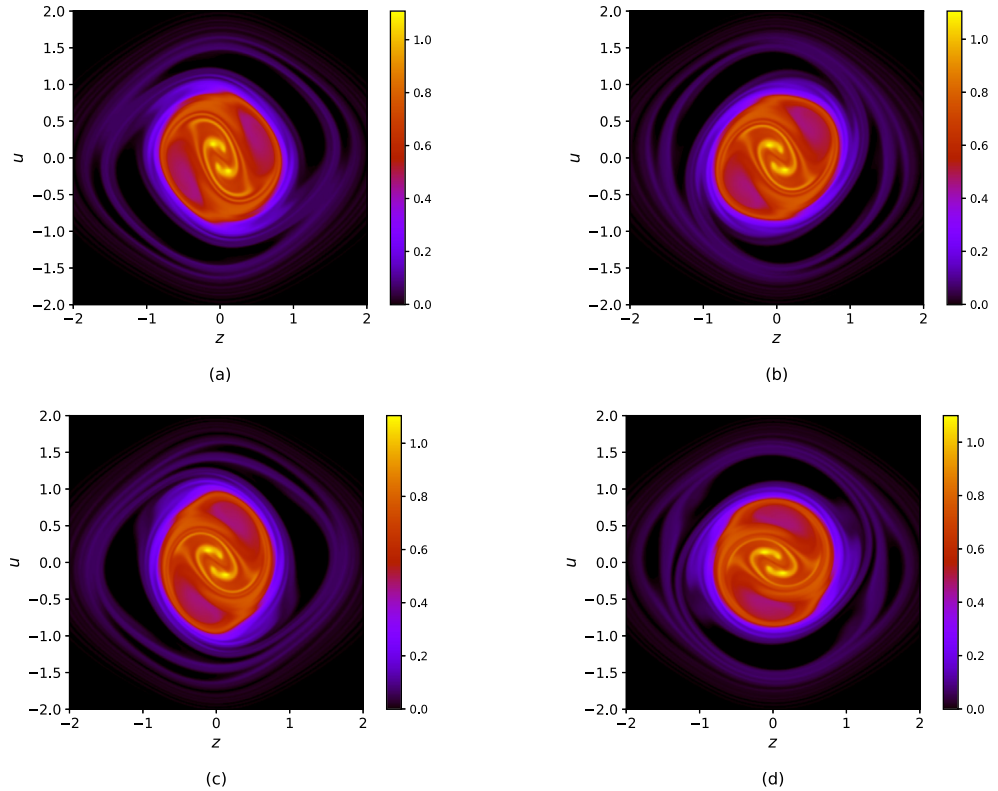

Figure 14. Phase density for $\alpha^2 = 0.5$ at $t/P = 85.217$ (a), 86.712 (b), 88.207 (c), and 89.702 (d).

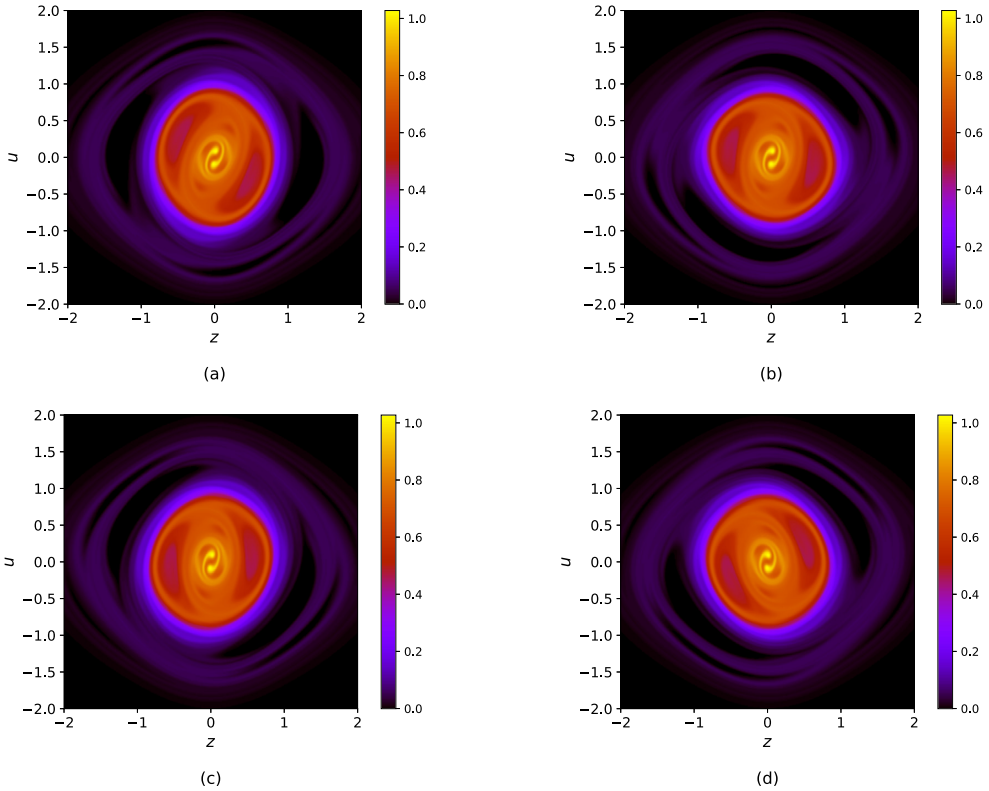

Figure 15. Phase density for $\alpha^2 = 0.5$ at $t/P = 174.919$ (a), 176.414 (b), 177.909 (c), and 179.404 (d).

6 CONCLUSIONS

In this work:

(i) A one-parameter model of a pulsating homogeneous self-gravitating layer is constructed with the same total energy and different amplitudes of the pulsations. The amplitude is determined by the virial relation averaged over the period that characterizes the degree of non-stationarity of the gravitating system.

(ii) The linear stability of this model with respect to large-scale perturbations was investigated and the critical value of the parameter characterizing the non-stationarity of the layer at which the instability occurs is found.

(iii) Numerical simulations based on the Vlasov–Poisson equations with initial distribution functions with values of the parameter near the critical one were performed. In the numerical simulations a high-resolution scheme which is the fifth-order conservative semi-Lagrangian WENO scheme is used. Results of the numerical simulations show that, for the unperturbed models, numerical and analytical solutions are in perfect agreement. The numerical solutions are highly sensitive to large-scale perturbations.

(iv) The development of large-scale perturbations imposed on a large-amplitude pulsating solution is simulated. In this case the spatial density approaches a stationary state, which indicates collisionless relaxation, approximately for the time interval of 200 pulsations.

According to results of the current research, we propose an approach to numerical simulation of the evolution of collisionless self-gravitating systems based on the use of exact analytical non-stationary solutions of the Vlasov–Poisson equations. These solutions can serve as benchmarks for validating numerical methods and verifying their software implementations. The stability regions of analytical solutions, especially multiparameter ones, can help when planning numerical experiments on the evolution of real stellar systems. We hope in the future to extend this work to the multidimensional case. There are a number of exact solutions in the 4D and 6D phase space obtained in papers such as Antonov & Nuritdinov (1981), Malkov (1986a,b), Vietri (1990), Nuritdinov (1995), and Malkov (2001), which can be used for validating numerical solvers. A preliminary discussion of these solutions as candidates for benchmarks is given in Malkov & Nuzhnova (2003).

ACKNOWLEDGEMENTS

This work was supported by the Russian Science Foundation (Project No. 18-11-00246), which is gratefully acknowledged. All computations were performed on the hybrid cluster of the Novosibirsk State University (http://nusc.nsu.ru/).

REFERENCES

Alard C., Colombi S., 2005, MNRAS, 359, 123
Antonov V. A., 1971, Trudy Astron. Obs. Leningrad Univ., 28, 64
Antonov V. A., Nuritdinov S. N., 1981, SvA, 25, 659
Arad I., Lynden-Bell D., 2005, MNRAS, 361, 385
Arber T. D., Vann R. G. L., 2002, J. Comput. Phys., 180, 339
Arnold V. I., 1989, Mathematical Methods of Classical Mechanics, 2nd edn. Springer, New York
Binney J., Tremaine S., 2008, Galactic Dynamics, 2nd edn. Princeton Univ. Press, Princeton, NJ
Camm G. L., 1950, MNRAS, 110, 305
Carillo J. A., Vecil F., 2007, SIAM J. Sci. Comput., 29, 1179
Cheng S. Z., Knorr G., 1976, J. Comput. Phys., 22, 330
Colombi S., Alard C., 2017, J. Plasma Phys., 83, 705830302
Colombi S., Touma J., 2014, MNRAS, 441, 2414
Colombi S., Sousbie T., Peirani S., Plum G., Suto Y., 2015, MNRAS, 450, 3724
Crouseilles N., Respaud T., Sonnendrücker E., 2009, Comput. Phys. Commun., 180, 1730
Crouseilles N., Mehrenberger M., Sonnendrücker E., 2010, J. Comput. Phys., 229, 1927
Filbet F., Sonnendrücker E., 2003, Comput. Phys. Commun., 150, 247
Filbet F., Sonnendrücker E., Bertrand P., 2001, J. Comput. Phys., 172, 166
Fridman A. M., Polyachenko V. L., 1984, Physics of Gravitating Systems I. Springer, New York
Hahn O., Angulo R. E., 2016, MNRAS, 455, 1115
Halle A., Colombi S., Peirani S., 2019, A&A, 621, A8
Iooss G., Joseph D. D., 1980, Elementary Stability and Bifurcation Theory. Springer, New York
Joyce M., Worrakitpoonpon T., 2011, Phys. Rev. E, 84, O11139
Kalnajs A. J., 1973, ApJ, 180, 1023
Lynden-Bell D., 1967, MNRAS, 136, 101
Malkov E., 2001, in Deiters S., Fuchs B., Spurzem R., Just A., Wielen R., eds, ASP Conf. Ser.Vol. 228, Dynamics of Star Clusters and the Milky Way. Astron. Soc. Pac., San Francisco, p. 67
Malkov E. A., Nuzhnova T. N., 2003, Astron. Astrophys. Trans., 22, 237
Malkov E. A., 1986, Astrophysics, 24, 221
Malkov E. A., 1986, Astrofizika, 24, 416
Mocz Ph., Succi S., 2017, MNRAS, 465, 3154
Nakamura T. K., 2000, ApJ, 531, 739
Nuritdinov S., 1995, Astron. Astrophys. Trans., 7, 307
Qiu J.-M., Christlieb A., 2010, J. Comput. Phys., 229, 1130
Qiu J.-M., Shu C.-W., 2011, Commun. Comput. Phys., 10, 979
Rocha Filho T. M., 2013, Comput. Phys. Commun., 184, 34
Sonnendrücker E., Roche J., Bertrand P., Ghizzo A., 1999, J. Comput. Phys., 149, 201
Sousbie T., Colombi S., 2016, J. Comput. Phys., 321, 644
Strang G., 1968, SIAM J. Numer. Anal., 5, 506
Syer D., Tremain S., 1995, MNRAS, 276, 467
Tanaka S., Yoshikawa K., Minoshima T., Yoshida N., 2017, ApJ, 849, 76
Theis C., 1998, A&A, 330, 1180
Trenti M., Hut P., 2008, preprint (arXiv:0806.3950)
Umeda T., 2008, Earth Planet. Space, 60, 773
Vietri M., 1990, MNRAS, 245, 40
Yamaguchi Y. Y., 2008, Phys. Rev. E, 78, 041114
Yoshikawa K., Yoshida N., Umemura M., 2013, ApJ, 762, 116

This paper has been typeset from a TEX/LATEX file prepared by the author.